

Minimum Requirements for Detecting a Stochastic Gravitational Wave Background Using Pulsars

J. M. Cordes

Astronomy Department, Cornell University

`cordes@astro.cornell.edu`

and

R. M. Shannon

Astronomy Department, Cornell University; CSIRO Astronomy and Space Science, Epping, NSW, 1710, Australia

`ryans@astro.cornell.edu`

ABSTRACT

We assess the detectability of a nanohertz gravitational wave (GW) background with respect to additive white noise and especially red noise in the timing of millisecond pulsars. We develop detection criteria based on the shape and amplitude of the cross-correlation function summed over pulsar pairs in a pulsar timing array. The distribution of correlation amplitudes is found to be non-Gaussian and highly skewed, which significantly influences the detection and false-alarm probabilities. When only white noise combines with GWs in timing data, our detection results are consistent with those found by others. Red noise, however, drastically alters the results. We discuss methods to meet the challenge of GW detection (“climbing mount significance”) by distinguishing between GW-dominated and red or white-noise limited regimes. We characterize plausible detection regimes by evaluating the number of millisecond pulsars that must be monitored in a high-cadence, 5-year timing program for a GW background spectrum $h_c(f) = Af^{-2/3}$ with $A = 10^{-15} \text{ yr}^{-2/3}$. Our results suggest that unless a sample of 20 super-stable millisecond pulsars can be found — those with timing residuals from red-noise contributions $\sigma_r \lesssim 20 \text{ ns}$ — a much larger timing program on $\gtrsim 50 - 100$ MSPs will be needed. For other values of A , the constraint is $\sigma_r \lesssim 20 \text{ ns} (A/10^{-15} \text{ yr}^{-2/3})$. Identification of suitable MSPs itself requires an aggressive survey campaign followed by characterization of the level of spin noise in the timing residuals of each object. The search and timing programs will likely require substantial fractions of time on new array telescopes in the southern hemisphere as well as on existing ones.

1. Introduction

There is current strong interest in exploiting the spin stability of millisecond pulsars (MSPs) to detect gravitational waves (GWs) at nanohertz frequencies ($\sim 0.1 - 1 \text{ cy yr}^{-1}$). Sources of GWs in this band include mergers of supermassive black holes that collectively produce an isotropic background

(Jaffe & Backer 2003; Phinney 2004; Jenet et al. 2005; Sesana et al. 2008) and in a few cases may be detected individually (Lommen & Backer 2001; Jenet et al. 2004; Finn & Lommen 2010; Yardley et al. 2010). Timing may also detect GW backgrounds from cosmic strings (Ölmez et al. 2010), the influence of massive gravitons (Lee et al. 2010), or solar system perturbations from primordial black holes (Seto & Cooray 2007). Detection methods have been based on finding excess variance in the timing residuals of individual sources, investigating spectral signatures in power spectra, or identifying the angular correlation expected between pulsar pairs from GWs passing through the solar system. Astrophysical and instrumental processes limit the timing precision of any given pulsar and the overall sensitivity of a pulsar timing array (PTA).

However, the efficacy of detection methods has received very uneven assessment with respect to contamination from different kinds of additive noise. These include both white and red noise processes, the latter having power strongly concentrated at lower fluctuation frequencies. We evaluate their impact on the sensitivity to a stochastic GW background, which itself comprises a red noise process.

In this paper, we are concerned with *detection* of GWs as distinguished from their detailed characterization. Recent work has considered both frequentist (e.g. Jenet et al. 2005; Yardley et al. 2011) and Bayesian approaches (e.g. van Haasteren et al. 2009, 2011) to the detection problem. While these methods are robust to varying degrees, our view is that detection needs to be corroborated with convincing diagnostics. We draw an analogy with the detection of a new spectral line or detection of cosmic microwave background fluctuations. Bayesian inference can yield the best probabilistic constraints on signal parameters, but most observers are convinced of an underlying detection and characterization only with the display of a spectral line or the power vs. spherical harmonic number that indicates a significant signal with respect to measurement errors. The corresponding quantity in the pulsar-GW problem is the cross correlation between the timing residuals of pulsar pairs or some related quantity.

We derive a general expression for the signal-to-noise ratio (SNR) of a correlation-based detection statistic and develop a detection protocol based on the shape and amplitude of the cross-correlation function. We assess the challenges for a likely detection and estimate the minimum number of MSPs needed under different circumstances. To do so, we consider a hypothetical pulsar distribution that yields the highest possible SNR for the correlation function, all else being equal. This is a configuration where N_p pulsars are in the same direction but at different distances so that the perturbation from GWs passing through the solar system is 100% correlated between all objects. Any other configuration will yield smaller correlation and SNR.

The correlated effect on times of arrival (TOAs) for different pulsars is produced by GWs passing through the solar system (Hellings & Downs 1983). We designate the Hellings and Downs angular correlation function as $\zeta(\theta)$ for two objects separated by an angle θ , with normalization $\zeta(0) = 1$; this differs from other definitions in the literature that include a delta function associated with GWs at the pulsar location, which yields $\zeta(0^+) = 1/2$. For our purposes, we keep the pulsar term separate.

We assess detectability in terms of different levels of white and red noise in timing residuals. Our work follows Cordes & Shannon (2010) where we assess a wide range of contributions to TOA errors from the pulsar, the interstellar medium, and from instrumental effects. White noise not

only includes radiometer noise but also pulse-to-pulse phase jitter from magnetospheric activity and from an effect associated with interstellar scintillation, which are pulsar and line-of-sight (LOS) dependent, respectively. We have also shown that red spin noise, which is common in canonical pulsars — those with periods of order one second and surface magnetic fields $\sim 10^{12}$ G — is also to be expected in MSPs but at low levels in accord with their spin parameters (Shannon & Cordes 2010). Interstellar scintillation also contributes red-noise TOA perturbations, some of which can be corrected before any analysis for GWs.

In the next section we describe the cross correlation analysis of a simplified timing model and develop detection criteria for assessing the presence of a GW signal. In § 3 we describe how the prospects for detection can be maximized. We summarize our results and discuss them in broader terms in § 4. The Appendix defines quantities used to characterize the timing residuals and describes simulations.

2. Cross Correlation Detection

We use a simplified model for the timing residuals of a pulsar by excluding real-world effects such as time transfer and the error in the location of the solar-system barycenter (e.g. Backer & Hellings 1986).

$$x(t) = e(t) + u(t), \quad (1)$$

where $e(t)$ is the “Earth” part of the gravitational wave (GW) background and $u(t)$ includes all other processes, which we assume are uncorrelated between different pulsars. At minimum, $u(t)$ includes the GW perturbation $p(t)$ at the pulsar’s location that acted on the measured signal a time D/c earlier, where D is the pulsar’s distance. Later we expand $u(t)$ into three components that are uncorrelated with $e(t)$ and with each other,

$$u(t) = p(t) + r(t) + n(t), \quad (2)$$

where $r(t)$ is red noise associated with spin noise (“timing noise”) in the pulsar or with multipath propagation in the interstellar medium (ISM), and $n(t)$ is white noise that represents measurement errors of different kinds. Each is characterized by a correlation function $\sigma_x^2(T)\rho_x(t, t')$, where $\sigma_x^2(T)$ is the ensemble-mean variance over an interval $[0, T]$ and $\rho_x(t, t')$ is the normalized correlation function defined with two arguments to handle non-stationary as well as stationary processes.

Figure 1 (left panel) shows simulated time series for a 20-MSP PTA. The time series show the e terms to be identical for all 20 pulsars, as assumed, while the p and r terms are different. The sum of all terms and the residuals from a second-order polynomial fit are also accordingly different. The bottom row of the panel shows sums of the various terms in the first five columns, which demonstrate the reduction in rms by $1/\sqrt{20}$ for the p and r terms. In the right-hand panel CCFs for 20 realizations of the PTA are shown where the GW, red-noise and white-noise contributions are equal over the data span T , corresponding to $\psi = 1$ and $\sigma_e = \sigma_p = \sigma_r = \sigma_n$ in one set of curves (the left column), while the GWs are turned off for the curves in the right-hand column.

The model in Eq. (1)-(2) is a sum of Gaussian distributed processes because all terms originate from conditions that usually will satisfy the central limit theorem (CLT). Focusing events in the

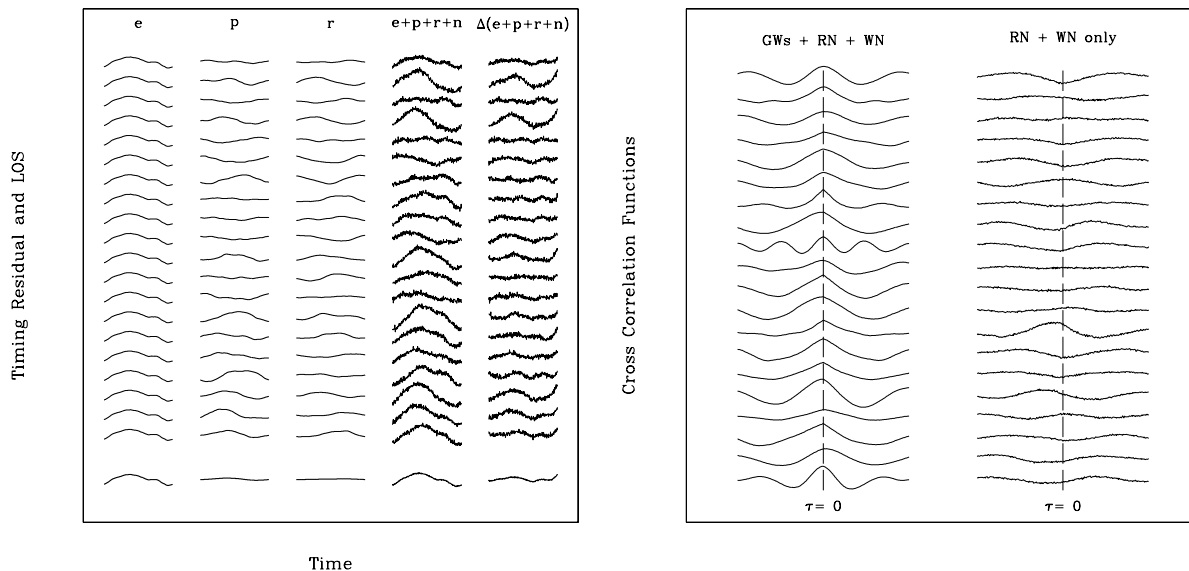


Fig. 1.— (Left) Simulated time series for a 20-pulsar timing array over 5 years. The columns from left to right show the e , p and r terms in the timing model, their sum added to white noise (n), and the residuals $\Delta(e+p+r+n)$ from a second-order polynomial fit. The simulations include GWs, red noise and white noise that have identical rms values $\sigma_{\text{gw}} = \sigma_r = \sigma_n = 20$ ns. in the post-fit time series. The bottom row shows the average of each column over the 20 pulsars. (Right) CCFs for a 20-pulsar PTA after removing a quadratic fit to each residual time series before cross correlating between all pairs. The left-hand column shows results for 20 realizations of the PTA shown in the left-hand panel. The right-hand column shows cases with no GW contribution.

interstellar medium (Coles et al. 2010) or events intrinsic to the pulsar can plausibly induce non-Gaussian statistics in data from some objects. The cross-correlation between pulsars, being a second moment, is a sufficient statistic for the angular correlation function. We define the general temporal cross-correlation function (CCF) in the Appendix and focus attention here on its zero-lag value

$$\widehat{C}_{00} \equiv \widehat{C}(\theta = 0, \tau = 0) = \frac{1}{N_X} \sum_{i < j} \widehat{C}_{ij}(\theta_{ij} = 0, \tau = 0) = \frac{1}{N_X T} \sum_{i < j} \int_0^T dt x_i(t) x_j(t), \quad (3)$$

which defines the single-pair CCF \widehat{C}_{ij} and the number of unique pairs in the double sum over i, j is $N_X = N_p(N_p - 1)/2$ for N_p pulsars. We have used continuous time notation; we justify this in the Appendix where we also discuss how to treat discretely sampled data. The ensemble average is

$$\langle \widehat{C}_{00} \rangle = \left\langle T^{-1} \int_0^T dt e^2(t) \right\rangle \equiv \psi \sigma_{\text{gw}}^2(T). \quad (4)$$

We use ψ to denote the ratio of the variances of the actual Earth term and the ensemble average variance. For red processes with power-law spectra $\propto f^{-y}$, the range of ψ covers one to a few orders

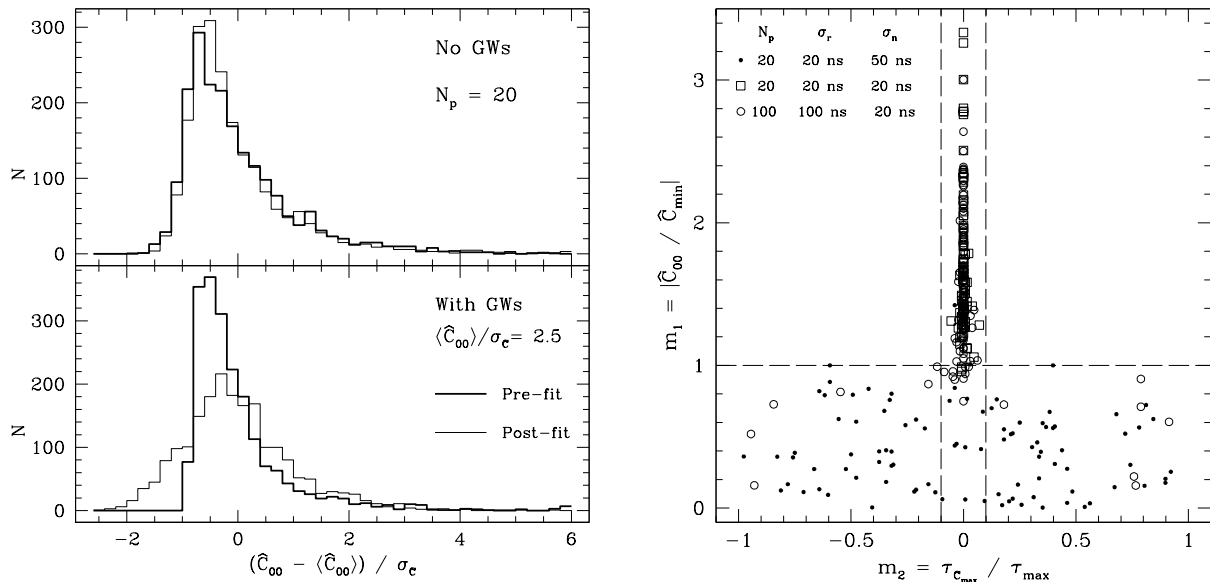


Fig. 2.— (Left) Histograms of the zero-lag values of cross-correlation functions based on simulations of PTAs that use 20 pulsars. The mean of 2000 realizations is subtracted from each value and the result is normalized by the rms deviation, $\sigma_{\hat{C}}$. Heavy lines show the histogram of \hat{C}_{00} calculated using the pre-fit time series and the light lines show post-fit results. In the top panel GWs do not contribute to the timing residuals while in the bottom panel they contribute $\sigma_{\text{gw}} = 20$ ns after a polynomial fit. Uncorrelated red and white noise contribute post-fit rms values $\sigma_r = \sigma_n = 20$ ns to each time series. Note that the histograms in the bottom panel have been shifted by the average, post-fit signal to noise ratio, which for this case is $S = \langle \hat{C}_{00} \rangle / \sigma_{\hat{C}} = 2.5$, where $\sigma_{\hat{C}}$ is calculated from the simulations. The histograms in the upper panel have $\langle \hat{C}_{00} \rangle = 0$. (Right) Plot of metrics m_1 vs. m_2 that characterize the shape of the cross correlation function of the post-fit timing residuals, as defined in the text; points are shown for 100 realizations of each case. The dashed lines denote the minimum threshold for the vertical axis and the maximum departure of the CCF peak from zero lag in order to provide a plausible detection. The open circles are for a case with no GW contribution while the open squares and filled circles have a post-fit GW rms of 20 ns in each time series.

of magnitude, with steeper power laws showing a wider range, as discussed in the Appendix. This implies that the GW background yields an actual rms TOA perturbation that can vary by more than a factor of ten. We define the signal to noise ratio $S = \hat{C}_{00} / \sigma_{\hat{C}}$ in § 2.3. Our definition for S has some similarity to that defined by Jenet et al. (2005) but with a crucial difference. Their Eq. 4 is essentially a matched filter based on the Hellings and Downs angular correlation. In our notation, the numerator of their equation is (with subscript “J” for Jenet et al.)

$$\hat{C}_J = \frac{1}{N_X} \sum_{i < j} \left[\hat{C}_{ij}(\theta_{ij}) - \bar{C} \right] \left[\zeta_{ij} - \bar{\zeta} \right]. \quad (5)$$

The angular separation of the i -th and j -th objects is θ_{ij} and barred quantities are sample means

over all pulsar pairs of \hat{C}_{ij} and $\zeta_{ij} \equiv \zeta(\theta_{ij})$, respectively. The ensemble mean is

$$\langle \hat{C}_J \rangle = \sigma_{\text{gw}}^2 (\overline{\zeta^2} - \bar{\zeta}^2), \quad (6)$$

where

$$\overline{\zeta^n} = \frac{1}{N_X} \sum_{i < j} \zeta^n(\theta_{ij}). \quad (7)$$

For the compact pulsar configuration we consider, $\langle \hat{C}_J \rangle$ vanishes because $\overline{\zeta^2} = \bar{\zeta} = 1$ and thus cannot be used to quantify detection in this case. If we redefine the weighted correlation as

$$\hat{C}'_J = \frac{1}{N_X} \sum_{i < j} \hat{C}_{ij}(\theta_{ij}) \zeta_{ij}, \quad (8)$$

the Jenet et al. test statistic becomes

$$S'_J = \frac{\hat{C}'_J}{\sigma_{C'_J}}, \quad (9)$$

which is identical to our definition for S when the pulsar configuration is compact with $\theta_{ij} = 0$.

Later in the paper we will relate our results to an arbitrary configuration of pulsars by considering S'_J , which simply multiplies our result for S by the mean-square angular correlation over the sample, $\overline{\zeta^2}$.

2.1. Detection Criteria

Over an ensemble, the CCF vanishes unless there is a significant correlated term from the $e(t)$ term (or from errors in the location of the solar system barycenter or from instrumentation that we do not include in our analysis). However, deviations from ensemble-average statistics in real data will produce both false positive and false negative detections from the uncorrelated terms in the timing residuals, like those shown in Figure 1.

A detection protocol for GWs can exploit the following aspects of timing residuals and their correlations:

1. The timing residuals must include a red-noise process caused by one or more of the predicted isotropic GW backgrounds (Jenet et al. 2005). If GWs from any discrete source are significant, there should be a corresponding departure from white-noise statistics described by a spectrum that depends on the nature of the GWs (Lommen & Backer 2001).
2. The maximum of the CCF is at or near zero time lag, $\tau \approx 0$, depending on how strong the GWs are relative to other contributions. Uncorrelated contributions produce estimation errors in \hat{C}_{00} that peak at arbitrary time lags in estimates using a finite number of pulsars and thus can induce false non-detections and false positive detections.
3. The zero-lag amplitude of the CCF must be significantly larger than expected when only uncorrelated terms contribute to the time series.

4. The correlation between pulsars is consistent with that expected (e.g. Eq. 5 of Hellings & Downs, 1983) for an isotropic background or the equivalent angular correlation for a discrete source.
5. Any correlation established using one set of pulsars can be checked using a completely independent set of pulsars.

When white and red-noise processes are significant, the estimated CCF has a high probability of peaking at a non-zero time lag. If white noise dominates the timing residuals of all pulsars, the CCF itself will vary rapidly with time lag and its formal maximum could be at any lag. Red noise by definition has a long correlation time so the CCF can appear quite smooth and yet peak far away from the origin. After a second order polynomial fit, the red-noise residuals will typically have two zero crossings so the CCF maximum is likely to be more centered than the pre-fit CCF, an effect we see in simulations. Nonetheless, the full CCF provides important statistical tests of the zero lag value.

Figure 2 (left-hand panel) shows histograms of \widehat{C}_{00} obtained from simulations with and without a GW contribution and for both pre-and-post-fit cases. Under relevant circumstances, the distribution is asymmetric, with a long tail for positive values while the mode and median are less than the mean. This counterintuitive result, discussed in the Appendix, occurs when the correlated quantity includes a red process with a steep power spectrum. The time series for a red process is effectively dominated by approximately one independent fluctuation so that the calculation of the CCF for one pair of pulsars does not satisfy the requirements for the CLT to apply, as it would if the time series were only white noise. The sum over all pulsar pairs also does not satisfy the requirements in part because the number of pairs exceeds the number of individual objects. Simulations show that the distribution for \widehat{C}_{00} becomes increasingly skewed for steeper spectra and for larger N_p . We have not yet explored if there is an asymptotic form for the distribution. The skewness we have identified is similar in cause to that identified for studies of non-Gaussianity of temperature fluctuations in the cosmic microwave background (Smith et al. 2011).

The long tail influences the false-alarm rate significantly. One way to get a more symmetric distribution is to average multiple estimates of the cross correlation function. Multiple estimates can be obtained by subdividing timing residuals into M blocks, each of length T/M , as mentioned in (Shannon & Cordes 2010). The CLT will apply to the average so the distribution should tend to a Gaussian form. We discuss this further in § 2.3.

2.2. CCF Based Detection

We define two metrics that characterize the shape of the CCF,

$$m_1 = \left| \frac{\widehat{C}_{00}}{\widehat{C}_{\min}} \right|, \quad m_2 = \frac{\tau_{\widehat{C}_{\max}}}{\tau_{\max}}; \quad (10)$$

m_1 is the ratio of the CCF at zero lag to the most negative value; m_2 is the offset of the CCF maximum relative to the maximum calculated lag, which in our simulation is $\tau_{\max} = T/2$. The two metrics characterize the shapes of the CCFs without reference to the actual signal to noise ratio

of the GW signal and therefore provide a direct empirical mechanism for assessing the presence of a GW signal. We later define the signal to noise ratio S as an ensemble average quantity that can be related to physical models for the GWs. The metric m_1 is a similar measure but is based on a single realization of the correlation estimate and is normalized by the minimum of the particular CCF, not the rms value over an ensemble. Figure 2 (right panel) shows a scatter plot of m_1 and m_2 from simulations that displays a peak in m_1 near $\tau = 0$. The fraction of points in the peak depends on the strength of the GWs compared to other contributions and on the number of pulsars. For residuals dominated by uncorrelated red noise, there is a sizable fraction ($\sim 15\%$) of cases with peak values that can mimic a GW detection. We define a joint detection criterion that comprises a lower bound $m_1 > m_{1\min}$ and an upper bound $|m_2| \leq m_{2\max}$. We also define the detection fraction f_d as the fraction of PTA realizations in a simulation that satisfy the detection criteria. The corresponding false-alarm fraction is defined as the detection fraction in the absence of any GW signal.

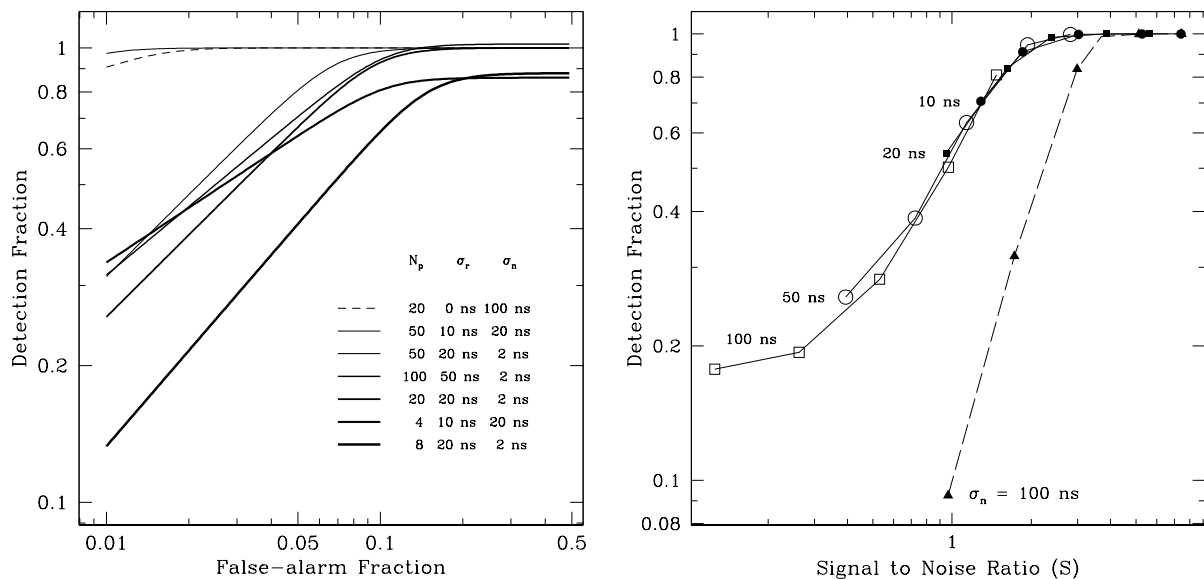


Fig. 3.— (Left) ROC curves showing detection fraction vs. false-alarm fraction for different detection criteria obtained by varying the thresholds for m_1 and m_2 . The detection fractions were calculated for the same GW strength (20 ns over 5 yr) but different numbers of pulsars and for different levels of red and white noise, as labeled. The false-alarm fraction was obtained by turning off the GW signal and keeping the red and white-noise levels the same as for the GW “on” case. (Right) Detection fraction plotted against the expected signal-to-noise ratio, S , of the cross correlation function. The five points for each curve correspond to PTAs with $N_p = 4, 8, 20, 50$ and 100 pulsars. Solid lines: The rms red and white noise are equal as labelled for each curve near the point corresponding to $N_p = 4$. Dashed line: A case with white noise with 100 ns rms (no red noise) added to the GW signal.

Inspection of Figure 2 suggests a threshold $m_{1\min} = 1$, which is plausible since the CCF of a noise-only signal is likely to have approximately equal positive and negative-going excursions. Also

consistent with the figure is a threshold $m_{2\max} = 0.1$, which enforces the zero time-lag nature of the “Earth” part of the GW signal but rejects cases where noise processes steer the CCF maximum away from zero lag.

The right-hand panel in Figure 1 shows cases where the CCFs satisfy the detection criteria (large amplitude and peak at $\tau = 0$) and others that do not. Conversely, when there is no GW contribution, red noise can cause false positive cases that satisfy the criteria. We quantify these features in the discussion that follows.

Specifying a detection criterion requires consideration of the tradeoff between the detection fraction, f_d , and the false-alarm fraction, f_{fa} . Figure 3 (left panel) shows “ROC” (receiver operating characteristics) curves calculated by varying $m_{1\min}$ and $m_{2\max}$ to alter the detection and false-alarm fractions. Each curve corresponds to a particular PTA (number of pulsars and levels of red and white noise). Ideally, one would like to have 100% detection fraction with no false alarms. The cases $(N_p, \sigma_r, \sigma_n) = (50, 10 \text{ ns}, 20 \text{ ns})$ and $(N_p, \sigma_r, \sigma_n) = (20, 0 \text{ ns}, 100 \text{ ns})$ come closest to this ideal. All of the other cases, which have larger noise levels or smaller numbers of pulsars in the PTA depart significantly from the ideal. With 20 pulsars having 20 ns of red noise and negligible white noise, a 90% detection fraction comes at the expense of a 11% false-alarm fraction. A larger number of pulsars (such as 50 pulsars with 20 ns red noise or 100 pulsars with 50 ns of red noise) decreases the false-alarm fraction to 8%.

The mapping of signal-to-noise ratio S and detection fraction is shown in Figure 3 (right panel). Most of the curves shown are for equal levels of red and white noise and different pulsar numbers (solid curves). Detection fractions $f_d \gtrsim 0.8$ require $S > 1.5$ and $f_d \gtrsim 0.95$ requires $S \gtrsim 2$. A case with 100 ns white noise (dashed curve) shows that $N_p = 20$ pulsars yields $S \approx 3$ and a detection fraction $> 80\%$ and minimal false-alarm fraction as shown in the left-hand panel. Our results are therefore broadly consistent with those of Jenet et al. (2005), who consider only white noise TOA errors. The primary conclusion from Figure 3 is that red noise drastically alters the detection and false-alarm fractions and therefore also any assessment of GW detectability.

2.3. SNR of the Zero-lag Cross Correlation

The detection criteria defined above are based solely on the shape of the cross-correlation function. It is useful to relate the detection fraction to the ensemble-average SNR of the correlation function (at zero lag), because the SNR can be related to the GW spectrum and properties of the PTA. The SNR of the CCF is defined as

$$S = \frac{\widehat{C}_{00}}{\sigma_{\widehat{C}}} = \frac{\psi\sigma_{\text{gw}}^2}{\sigma_{\widehat{C}}}, \quad (11)$$

where the rms variation $\sigma_{\widehat{C}}$ is given in the Appendix and includes the contributions from the GWs themselves along with uncorrelated red and white noise. For arbitrary combinations the SNR is

$$S = \frac{\sqrt{\psi N_p M}}{2} \left\{ w_{gg} + \xi_M w_{rr} + \frac{(w_{gg} + \xi_M^2 w_{rr} + 2\xi_M w_{gr})}{2\psi(N_p - 1)} + \frac{\eta_M M}{N_t} \left[1 + \frac{(\eta_M/N_s + 2 + 2\xi_M)}{2\psi(N_p - 1)} \right] \right\}^{-1/2} \quad (12)$$

Simulations yield SNRs that agree with this expression to within statistical errors. In Eq. (12) we have allowed for the division of the full time series into M blocks and incoherent averaging of the

CCF for each block, reducing the variance by $1/M$. Both σ_u and σ_{gw} depend implicitly on M , as discussed below. The SNR depends on rms red and white noise levels through the variance ratios $\eta_M = \sigma_n^2/\sigma_{\text{gw}}^2$ and $\xi_M = \sigma_r^2/\sigma_{\text{gw}}^2$ that depend on the time span T/M owing to the nonstationarity of the red noise and GW signals. The number of blocks also enters in the leading coefficient in Eq. (12), because the correlation estimate from each block is averaged and we assume that the estimates are statistically independent. We have verified that red processes with spectral indices of four or less show this statistical independence. For steeper spectra, there is some correlation between blocks.

For a dimensionless strain amplitude spectrum $h_c(f) = Af^{\alpha_g}$, the spectrum of timing residuals $\propto f^{2\alpha_g-3}$ and the rms residual scales as $\sigma_{\text{gw}}(T) \propto T^{x_g}$ with $x_g = 1 - \alpha_G$ for $\alpha_g < 1$. For the GW background produced by merging SMBHs (Jaffe & Backer 2003), $\alpha_g = -2/3$ and $x_g = 5/3$. We will use a fiducial value $A = 10^{-15} \text{ yr}^{-2/3}$. Similarly, red timing noise has been characterized with exponents $x_r \approx 2 \pm 0.2$ corresponding to a spectrum $\propto f^{-5 \pm 0.4}$ (Shannon & Cordes 2010). The dimensionless ratios then become $\eta_M = \eta_1 M^{2x_g}$ and $\xi_M = \xi_1 M^{2(x_g - x_r)}$, where η_1 and ξ_1 are the values for the full-length time series ($M = 1$).

The quantities w_{gg}, w_{rr} and w_{gr} are dimensionless correlation times that are defined in the Appendix. For steep power-law spectra, they are of order unity and independent of the data-span length owing to self-similarity. This same statement holds whether we consider the timing residual model in Eq. (1) to represent pre-fit residuals or those after removing a polynomial to account for corrections to the spin parameters. Inclusion of astrometric sinusoidal terms in the fitting function with one year and half-year periods will induce some dependence of the dimensionless scales on T but with diminishing importance as $T \gg 1 \text{ yr}$. The equivalent quantity for white noise is $1/N_t$ because adjacent samples are uncorrelated.

Smoothing (low-pass filtering) and decimation of the time series by N_s samples before correlation reduces the rms of the white-noise. We consider cases where $N_s \ll N_t/M$ so that with blocking there is still a large number of samples per block. We also consider the implied smoothing time $N_s T/N_t$ to be small enough that it does not reduce the variance of the red processes over the block length T/M .

The simplest case, though unrealizable, is where only GWs contribute to the timing residuals with the e term perfectly correlated and the p term completely uncorrelated. The SNR is

$$S = \frac{1}{2} \left[\frac{\psi N_p M / w_{gg}}{1 + 1/2\psi(N_p - 1)} \right]^{1/2} \approx \frac{1}{2} \sqrt{\frac{\psi N_p M}{w_{gg}}}, \quad (13)$$

the approximate equality holding when the number of pulsars is very large, $\psi N_p \gg 1$. The SNR grows as $\sqrt{N_p}$ and can become arbitrarily large with \sqrt{M} subject to the requirement that the continuum approximation holds for arbitrarily small T/M . When white noise or red noise contribute, however, there is a distinct maximum in S vs. M .

A number of other features are evident in Eq. (12), which has terms inside the curly brackets scaling as $\mathcal{O}(1), 1/N_p, 1/N_t$ and $1/(N_p N_t)$. The number of TOAs, N_t , is important only as long as the white noise part of the residuals is sizable. If less than other terms, the number of TOAs — and thus any cadence in acquiring them — becomes unimportant. A larger number of pulsars can reduce the effects of both the red and white noise from non-GW contributions in addition to

reducing the uncorrelated “pulsar” part of the GWs. For very large N_t and N_p , the SNR reduces to that for the GW-only case.

We illustrate these and other trends in Figure 4. In the left panel, the SNR is plotted against the number of blocks for cases that include red and white noise added to the GW perturbation. The plotted values are based on $\psi = 1$ and on a total of $N_t = 10^3$ TOAs over five years for 100 pulsars. We have dimensionalized the values for η_M using $A = 10^{-15}$. After a second order fit to a $T = 5$ yr data span, the rms residual is $\sigma_{\text{gw}}(T) \approx 20$ ns (e.g. Shannon & Cordes 2010).

The curve for no noise (red or white) increases monotonically with M , but there is a distinct maximum SNR for non-zero noise that separates the GW dominated and noise dominated regimes. The optimal number of blocks is $M \approx 3$ to 6 for the cases shown. In the noise-dominated regime, the SNR scales as $\psi N_p \sqrt{N_t N_s} M^{-2x_g}$, so smoothing improves the SNR but blocking does not. When the SNR is not noise limited, it no longer depends on N_t , so smoothing will have no effect. This may be seen in Figure 4 (left panel) for the curves labeled 20, 50 and 100 ns which converge at high SNR for both smoothing values shown, $N_s = 1$ and 30. In the GW dominated case, there is no dependence on N_t , N_s , or on the scaling exponent, x_g .

Figure 4 (right panel) shows the SNR plotted against the number of pulsars used for several different values of white and timing noise. The curves in the figure were calculated for $M = 3$ blocks and using a red noise scaling $\sigma_r \propto T^{x_r}$ with $x_r = 2$. If red spin or ISM noise is absent ($\xi_M = 0$), $S \propto \sqrt{N_t N_p}$ for $S \ll 1$ is linear in the number of pulsars (for large N_p) but then has a shallower dependence $S \propto \sqrt{N_p}$ when S is large enough to provide a confident detection. If we let S_{gw} be the SNR for the GW-only case in Eq. (13), it can be shown that $S \ll S_{\text{gw}}$ in the white-noise limited case where the η_M^2 dominates other terms in Eq. (12) and $S \propto N_p/\eta_M$. Thus for S large enough to correspond to a plausible detection, it is not likely to scale with N_p as it does in the noise-limited regime but instead will scale as $S \propto \sqrt{N_p}$.

2.4. Comparison with Other Detection Approaches

Our method uses the CCF as a test statistic and we calibrate it against the SNR S that can be related to theoretical GW spectra and sources of noise. Our expression for S in Eq. (12) is similar to Eq. (12) of Jenet et al. (2005), who define their detection significance as the SNR S_J of a weighted correlation quantity, as discussed in § 2. However, their expression does not explicitly account for red and white noise individually; instead a quantity χ is defined that measures the degree of whiteness of the timing residuals. Any non-white components are assumed to arise solely from the GW background and not from any additional spin-noise or ISM contribution. As a consequence, we do not expect the expressions for S and S_J to yield the same values for the same PTAs. In addition, it is assumed that S_J has Gaussian statistics when there is no GW contribution, with a false-alarm fraction calculated accordingly. As we have shown, if red-noise contributes to timing residuals, the distribution of S is highly non-Gaussian both with or without a contribution from GWs.

It is still instructive to compare nominal SNR values. For a pulsar timing array comprising $N_p = 20$ pulsars observed $N_t = 250$ times over $T = 5$ years with an rms error $\sigma_n = 100$ ns and no red noise, Jenet et al. (2005) (their Figure 1) find $\text{SNR} \approx 2.8$ for a GW background of the same

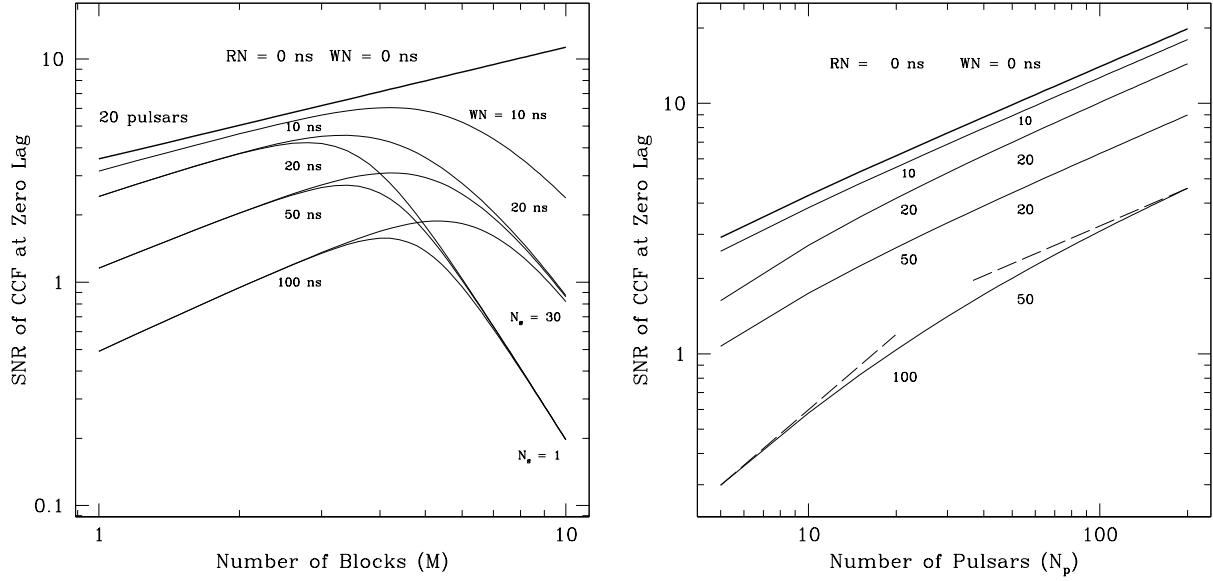


Fig. 4.— (Left) SNR of the cross-correlation function *versus* number of blocks for cases where the timing residuals include red noise from spin variations and/or ISM perturbations along with GWs and white noise. The plotted curves use $\sigma_r \propto T^{x_r}$ with $x_r = 2$ and are labeled with the values for $T = 5$ yr. For the six curves with 20 ns of white noise, three incorporate smoothing of $N_s = 30$ samples and the other three have no smoothing ($N_s = 1$). (Right) SNR of the cross-correlation function *versus* the number of pulsars in the timing array sample. Both red noise and white noise are included, as indicated. Dashed lines indicate $\text{SNR} \propto N_p$ and $\text{SNR} \propto N_p^{1/2}$, which are the asymptotic scaling laws at low and high SNR, respectively. The plotted curves assume that $\sigma_r \propto T^{x_r}$ with $x_r = 2$ and were calculated for $M = 3$ blocks and $N_t = 10^3$ data points.

form we have considered with $A = 10^{-15} \text{ yr}^{-2/3}$. For the same PTA we find $S = 2.9$ for $M = 1$. Jenet et al. (2005) obtain $S_J = 4.5$ using low-pass filtering (smoothing) and pre-whitening. Their low-pass filtering uses a high-frequency cutoff $f_{hc} = 4/T$, corresponding to $N_s = N_t/8$ in our notation. The blocking method we have analyzed shares some features similar to pre-whitening. Including smoothing and optimal blocking (which turns out to be $M = 1$ for this case), we obtain $S = 3.1$. As we have shown (Figure 3), this value is sufficient to yield a high detection fraction (~ 0.99) with a corresponding fairly low false-alarm fraction (0.02). Similar detection and false-alarm fractions are not available for the Jenet et al. (2005) approach. We note also that our values apply for the compact configuration of pulsars whereas those for Jenet et al. are for an unspecified configuration.

In a Bayesian treatment of GW detection, van Haasteren et al. (2009) cast detection in terms of parameter estimation and define the detection significance for the coefficient A of the GW spectrum using the SNR of A , μ/σ , which we denote as S_{vH} . For a PTA with $N_p = 20$, $T = 5 \text{ yr}$ and $N_t = 500$, their Figure 12 indicates $S_{\text{vH}} \approx 2$ and 4 for $\sigma_{\text{WN}} = 100 \text{ ns}$ and 50 ns , respectively. For the same cases, we find $S = 3.2$ and 3.8 , respectively, with no smoothing or blocking. van Haasteren & Levin (2010) state that their results are based on fixing all but one parameter (A) and thus yield larger than expected SNRs. We conclude that, nominally, our SNRs are not inconsistent with those of (van Haasteren & Levin 2010). We emphasize, however, that the most meaningful comparison is of detection and false-alarm fractions.

3. Climbing Mount Significance: Optimizing Detection

Methods for increasing the detection significance can be identified by using Eq. (12) in various limiting cases. In the white-noise limited regime, the composite quantity $Z_{\text{wn}} = N_p \sqrt{N_t N_s} / \sigma_n^2$ can be inspected. When red noise dominates the SNR, the quantity $Z_{\text{rn}} = N_p \sqrt{M} / \sigma_r^2$ is relevant. In the GW-dominated regime, we have $Z_{\text{gw}} = \sqrt{N_p M}$.

1. Increasing the number of pulsars N_p helps in any regime, though it has greater impact in the noise limited case (red or white). Detection of GWs almost certainly will occur in the regime where the SNR of the correlation-based detection statistic increases only as the square-root of the number of pulsars.
2. In the white noise-limited regime, increasing Z_{wn} through a combination of more pulsars, greater timing throughput, smoothing, and a decrease in timing error per TOA will increase S . A detection fraction larger than 0.9 combined with a false-alarm fraction $\lesssim 0.1$ requires $S \gtrsim 2$.
3. Because red noise is spectrally similar to the GW contribution and does not average out significantly in the CCF because of its long correlation time, the primary means for increasing the SNR is to sum over many pulsars and to use blocking.
4. In the GW-dominated regime, increasing the blocking M and the number of pulsars N_p are the only options. As the figures show, M cannot be increased arbitrarily because eventually the rms noise in the interval T/M will overwhelm the GW signal, which decreases with smaller T .

The sensitivity of a PTA to GWs of course improves with total observing span. In the white noise dominated case, these improvements are the greatest, with $S \propto T^{2x_g+1/2} \propto T^{23/6}$. However, a detection cannot be made in this regime where S is small. In the regime where detections can be made, the longer observing span only enables a larger amount of sub-blocking so that $S \propto \sqrt{T}$.

Of the factors we have discussed, the contributions to red and white noise from interstellar refraction and diffraction (Coles et al. 2010; Cordes & Shannon 2010) can be partly mitigated by using higher frequencies and by appropriate fitting across wide bandwidths. Larger telescopes and bandwidths can minimize radiometer noise but will have no effect on jitter. Longer integration times are the only recourse for jitter but they also will minimize radiometer noise

The most difficult hindrance to overcome is red noise from spin variations and from any residual ISM effects that cannot be corrected. The range of red timing noise levels in MSPs is not known definitively but our recent assessment (Shannon & Cordes 2010) suggests that it is larger in objects with larger spin-frequency derivatives. Latent red noise may emerge in many MSPs when more sensitive and longer time-span observations are obtained. If so, greater timing throughput will be needed to time more MSPs as well as to increase the observing time per pulsar to reduce white noise sufficiently for detection.

3.1. Implications

The GW dominated regime provides the largest SNR and thus indicates the absolute minimum number of pulsars needed to make a detection. Defining a threshold $S > S_{\min}$, the number of pulsars required is

$$N_p \geq 4S_{\min}^2 w_{gg} / \psi M. \quad (14)$$

For $\psi = 1$, $M = 1$, and $w_{gg} = 0.4$ a minimum SNR of 2 requires $N_p = 6$ pulsars, as seen in Figure 4. With no timing noise or white noise, M can be made arbitrarily large (subject to sampling rates). However, even optimistic values of white noise and red noise (e.g. 20 and 20 ns, respectively) indicate that S is maximized for $M \approx 2$ to 3, so $N_p \gtrsim 7/\psi$ is needed for $M = 3$. The actual variance of the “Earth” part of the GW background could have ψ much larger or smaller than unity, so detection of GWs with a small number of pulsars may be marginal. A larger threshold $\text{SNR}_{\min} = 5$ will require $N_p \gtrsim 25/\psi$ for $M = 3$. Our results suggest that an increase in the cadence of timing measurements to increase the total number of TOAs for each object (N_t) may be a necessary but insufficient course to take for GW detection.

To obtain our results, we have assumed that the Earth term $e(t)$ is the same for all pulsars in a hypothetical spatial configuration. For realistic distributions of pulsars on the sky, the correlation amplitude will be reduced by $\overline{\zeta^2} \approx 0.6$, thus increasing the number of required pulsars by about a factor of $1/(\overline{\zeta^2})^2 \approx 3$. For PTAs with a range of red-and-white-noise levels, weights for each pulsar can be introduced in the double sum in Eq. (3). For a nominal level of white noise, for example, with some objects having smaller and others larger rms values, a weighted sum will yield a larger SNR than the case where all objects have the same rms white noise. If we take the nominal value as the *minimum* in the sample, however, the optimally weighted \hat{C} will have lower SNR.

Currently only two MSPs (J1713+0747, J1909–3744) are known to have rms timing residuals less than 50 ns over a 5-yr interval (Demorest et al. 2009) and one other less than 100 ns, J0437–4715 (Manchester 2010). An aggressive campaign is needed to find more MSPs with timing noise substantially less than 100 ns in a 5-year span. The timing noise scaling law of Shannon & Cordes (2010) suggests that such MSPs will have small spindown rates and they may be less luminous if the radio beam luminosity correlates with the energy loss rate. This implies that MSP surveys may need to be more sensitive than at present.

The best strategy is to identify ~ 20 “super”-stable MSPs with rms timing noise of 20 ns or less over time spans of 5 years or more if a detection threshold $S_{\min} = 2$ is considered sufficient for detection. A larger $S_{\min} = 5$ requires ~ 50 objects. However, if no such super-stable objects exist and MSPs more typically have 20 ns rms timing noise or larger over 5 years, many more MSPs will need to be timed, perhaps exceeding 100 MSPs.

Even if the super-stable regime applies, once a detection is made, possibly using existing telescopes to time known stable objects along with any new discoveries in the near term, a more detailed analysis of the GW spectrum will be desired and that certainly will require a much larger set of MSPs and overall greater throughput of the timing.

Each MSP needs a careful error budget analysis. This would include a detailed characterization of the red and white noise levels, including a breakdown of each from different physical causes. The two kinds of noise can be distinguished through appropriate use of the structure function of timing residuals (e.g. Cordes & Downs 1985). Departures from white noise need to be characterized according to amplitude and spectrum and classified as contributions from red noise of any kind, from changes in instrumentation, which can cause jumps in pulse phase between epochs. A change-point analysis (e.g. Ó Ruanaidh & Fitzgerald 1996, Chapter 5) on timing residuals can identify the amplitudes of such jumps whether or not their occurrence epochs are known. MSPs with significant red noise that is demonstrated to be from non-GW causes should be rejected because they do not contribute to the sensitivity of a PTA to a stochastic background of GWs.

4. Discussion

The main results of our paper are as follows.

The cross-correlation function is the primary statistic that we consider for a hypothetical pulsar distribution that yields the maximum possible signal to noise ratio, all else being equal. For a realistic distribution, the equivalent quantity would be a weighted sum similar to the quantity ρ defined by (Jenet et al. 2005), but with a time-lag argument included. The CCF has amplitudes over an ensemble that have a positive skewed distribution that influences the detection and false-alarm fractions. We have taken this into account in our analysis and we also suggest that subdividing the entire span of timing residuals into $M \approx 3$ sub-spans for each pulsar will reduce the skewness and increase the statistical significance. Such blocking is equivalent to high-pass filtering the data. It requires a large-enough cadence for TOA measurements that there is an ample number of samples within each interval of length T/M .

The number of pulsars needed for a likely detection of nanohertz GWs depends strongly on the levels of white noise and especially the red noise in the data. In related papers (Cordes & Shannon

2010, Shannon & Cordes, in preparation) we have shown that both kinds of noise are likely to be present due to torque noise in the pulsar, magnetospheric motions of emission regions, and interstellar plasma phenomena.

Red and white noise timing residuals dramatically alter the achievable signal to noise ratio of the CCF. When residuals are white noise dominated, improvements can be made by increasing the net integration time per pulsar or by smoothing individual measurements over a time shorter than the smallest GW period that is likely to be identified. Marginal gains can also be made from blocking of the data.

If, however, the detection statistic is dominated by red noise with a power spectrum similar to that of the GW power spectrum, smoothing or other increases in net integration time per TOA will not help. The best recourse is to increase the number of pulsars in the pulsar timing array.

We have shown that the correlated GW signal contributes variance that can differ markedly from the ensemble value if the GW signal has a steep power-law spectrum, like that expected from merging of supermassive black holes. This stochasticity of the sample variance can either greatly enhance or diminish the chances of detecting the signal. The skewness of the correlation function's signal to noise ratio is an important factor in assessing detection and false-alarm statistics. The skewness is reduced when time series are divided into sub-blocks that are analyzed separately and then combined.

As mentioned in the previous section, an important action is the characterization of the timing error budget for each MSP.

We consider it likely that 50 to 100 spin-stable MSPs are needed to fully characterize GWs at nanohertz frequencies, including a secure detection followed by detailed characterization. A minimum of 20 MSPs is needed for a plausible detection under optimistic red and white noise levels, as described in this paper. A sample that is distributed on the sky will increase this number by $\sim 60\%$ and verification with a completely independent sample will require another doubling. The program going forward therefore requires an aggressive search campaign to discover more MSPs and to identify the most spin-stable objects. It is possible that the most stable objects are also those with smaller radio luminosities. The scaling law for red noise identified by (Shannon & Cordes 2010) implies that objects with larger spin-down rates have larger noise levels. While not known for certain, the radio luminosity likely also is larger for these objects. In addition, further study of spin noise in MSPs is needed to ascertain whether it can be mitigated, as suggested by Lyne et al. (2010).

We thank members of the NANOGrav collaboration for useful comments on this work. Our work was supported by the NSF through a subaward to Cornell University from Partnerships for International Research and Education award 0968296 to West Virginia University.

A. Appendix

A.1. Definitions and Correlation Time Scales

The GW perturbations induced in a pair of pulsars are correlated according to their angular separation (Hellings & Downs 1983). Following Jenet et al. (2005) and others, we define an estimator for the angular and temporal correlation function as an integral over time and a sum over the $N_X = N_p(N_p - 1)/2$ unique pairs of pulsars,

$$\widehat{C}(\theta, \tau) = \frac{1}{N_X(\theta)} \sum_{i,j:\theta} \frac{1}{T} \int_0^T dt x_i(t)x_j(t + \tau), \quad (\text{A1})$$

where pairs are summed such that the separation angle θ_{ij} between the i^{th} and j^{th} pulsars is within an angular bin centered on θ . In practice, the time integral is a sum over discrete time series, but it is more useful for our analysis to use continuous notation. It is easy to collapse our continuous-time result to the discrete-time case as discussed below.

In the main text we discuss the zero-lag correlation $\widehat{C}_{00} = \widehat{C}(0, 0)$ and its signal-to-noise ratio, $S = \widehat{C}(0, 0)/\sigma_{\widehat{C}}$. For a general $u(t)$, the rms \widehat{C}_{00} is

$$\sigma_{\widehat{C}} = \frac{2}{\sqrt{N_p}} \left[\psi \sigma_{\text{gw}}^2 \sigma_u^2 w_{eu} + \frac{\sigma_u^4 w_{uu}}{2(N_p - 1)} \right]^{1/2}, \quad (\text{A2})$$

where $\psi \sigma_{\text{gw}}^2$ is the mean square of $e(t)$ over the time interval and $\psi \approx 1$ takes into account that $e(t)$ is a single realization of the GW process while we define σ_{gw}^2 to be the ensemble-average variance (see further discussion below). The uncorrelated noise u has variance σ_u^2 ; w_{eu} and w_{uu} are dimensionless correlation times of order unity that are discussed below. If there are no GWs, we substitute $\sigma_u^4 w_{uu} \rightarrow \sigma_r^4 w_{rr} + (\sigma_n^4 + 2\sigma_r^2 \sigma_n^2)/N_t$, where N_t is the number of discrete samples in $[0, T]$. Using additional dimensionless correlation times for the no-GW case, we obtain

$$\sigma_{\widehat{C}} = \frac{\sqrt{2}}{N_p(1 - 1/N_p)^{1/2}} \left(\sigma_r^4 w_{rr} + \frac{\sigma_n^4 + 2\sigma_r^2 \sigma_n^2}{N_t} \right)^{1/2}. \quad (\text{A3})$$

The rms correlation scales as the inverse of the number of pulsars and is independent of the number of time samples when the red noise dominates. When GWs are significant, the dependence on N_p is slower, for large N_p scaling as $\sigma_{\widehat{C}} \approx 2\sigma_{\text{gw}}^2 \sqrt{w_{ep}/N_p}$. We have verified these scaling laws using simulations with different combinations of white and red noise and number of pulsars.

For arbitrary combinations of GWs, red, and white noise, we expand $u = p + r + n$ and use corresponding variances and correlation functions to get

$$\sigma_{\widehat{C}} = \frac{2\sigma_{\text{gw}}^2 \sqrt{\psi}}{\sqrt{N_p M}} \left\{ w_{ep} + \xi_M w_{er} + \frac{(w_{pp} + \xi_M^2 w_{rr} + 2\xi_M w_{pr})}{2\psi(N_p - 1)} + \frac{\eta_M M}{N_t} \left[1 + \frac{(\eta_M/N_s + 2 + 2\xi_M)}{2\psi(N_p - 1)} \right] \right\}^{1/2} \quad (\text{A4})$$

The dimensionless time scales used in the expressions for $\sigma_{\widehat{C}}$ result from double integrals that comprise the variance of the correlation function,

$$w_{ab} = T^{-2} \iint_0^T dt dt' \rho_a(t, t') \rho_b(t, t'), \quad (\text{A5})$$

where the factors in the integrand are normalized correlation functions for individual terms defined in Eq. (2), $\rho_a(t, t')$, with $a = e, p, r, n$. The correlation functions have two arguments because most of the processes we consider have nonstationary-like statistics over finite time intervals. We have $\sigma_a^2(T) = T^{-1} \int_0^T dt \langle a^2(t) \rangle$ and $\rho_a(t, t') \equiv \langle a(t)a(t') \rangle / \sigma_a^2(T)$.

We account for the fact that $e(t)$ represents a single realization of the GW signal. Under the assumption that all pulsars in the sample are in the same direction, $e(t)$ is identical for all lines of sight. By contrast, the GW signal at each pulsar's location, $p(t)$, is different for each LOS so that a set of $N_p \gg 1$ pulsars samples a range of variances that are well represented by the ensemble average. Therefore we write

$$\sigma_e^2(T)\rho_e(t, t') \equiv \psi\sigma_p^2(T)\rho_p(t, t') \equiv \psi\sigma_{\text{gw}}^2(T)\rho_g(t, t'), \quad (\text{A6})$$

where ψ is the ratio of the realization variance to the ensemble variance for the GWs.

Even though $e(t)$ represents a single realization while the correlation estimator uses $N_p \gg 1$ independent realizations of $p(t)$, we approximate both as having the same correlation function and same dimensionless correlation time, w_{gg} . We therefore let $w_{ep} \approx w_{pp} \approx w_{gg}$ and $w_{er} \approx w_{pr} \approx w_{gr}$.

The white-noise correlation ρ_n decorrelates on a time scale of one sample in discretely sampled data. Therefore the factors w_{en}, w_{pn}, w_{rn} , and w_{nn} , all become $1/N_t$, the reciprocal of the number of time samples. This approach is a good representation of timing residuals with irregular, discrete sampling where N_t is large enough to sample adequately the red processes, including the GW signal.

In contrast to white noise, the steep red power spectra for e, p and r yield dimensionless time scales $\gg 1/N_t$. Using simulations like those described below we find $w_{ep} \approx 0.36$ for red noise created with an $f^{-13/3}$ spectrum after removal of a second order polynomial. For red noise consistent with timing noise in pulsars ($\propto f^{-5}$), we obtain $w_{er} \approx 0.44$. For a flat spectrum (white noise), we verify that $w_{nn} = 1/N_t$ to within statistical errors in simulations.

Eq. (A4) incorporates smoothing of the original time series by N_s samples and for blocking of the total data span of N_t samples into subintervals of N_t/M samples corresponding to a time interval T/M . Each subinterval is processed separately and the correlation estimates are summed, reducing the rms $\sigma_{\hat{C}}$ by a factor $1/\sqrt{M}$. Clearly, any smoothing and blocking must yield a net number of samples per subinterval to be large enough to allow for a polynomial fit. We have also used dimensionless variance ratios, $\eta_M = \sigma_n^2 / \sigma_{\text{gw}}^2(T/M)$ and $\xi_M = \sigma_r^2(T/M) / \sigma_{\text{gw}}^2(T/M)$. We have explicitly indicated that the variances for the GWs and red noise are functions of the data span length, T/M . We discuss these in detail in the main text.

Figure 1 shows histograms of the rms timing perturbations before and after fitting a quadratic function for processes with spectral indices $y = 2, 4, 6$ (which correspond roughly to random walks in spin phase, frequency and frequency derivative) and $y = 13/3$, the value expected from a GW background produced by merging supermassive black holes (SMBHs). Histograms are also shown for pure white noise ($y = 0$). The ratio of rms values equals $\sqrt{\psi}$ for the pre-fit case and is proportional to $\sqrt{\psi}$ for the post fit case. The ratio varies by more than an order of magnitude before fitting but covers a somewhat smaller range after fitting.

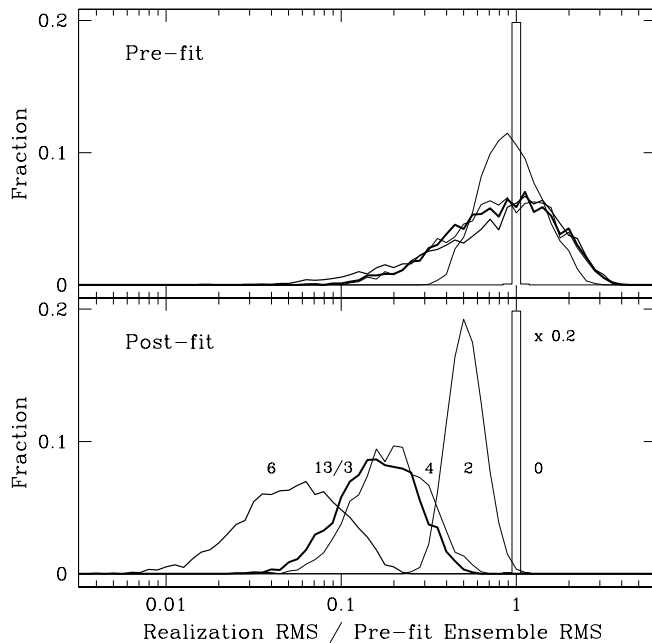


Fig. 1.— Histograms of the rms TOA for red processes with power-law spectra $\propto f^{-y}$ with $y = 0, 2, 4, 6$ and $13/3$, as labelled in the bottom panel. The top and bottom panels show results before and after removing a second-order polynomial. The rms values are normalized by the ensemble rms of the pre-fit time series.

A.2. Generation of Simulated Time Series

We generate realizations of red noise by shaping complex white noise in the frequency domain and performing an inverse discrete Fourier transform. We fill an array that includes Fourier components with periods that are four times longer than our desired time series so that low-frequency components are not underestimated. We then select $1/4$ of the time series. To suitably mimic the analysis of pulsar timing data, we subtract a straight line whose end points equal the first and last data points. This accounts for the fact that prior to doing a least-square fit to timing data, a preliminary timing model is first removed. In this way we compare pre-and-post fit variances that are close to representing those that would result in actual applications.

A.3. Non-Gaussianity of the Zero-lag CCF

In the main text we describe the skewness of the distribution of \widehat{C}_{00} toward positive values. The skewness is generic for time series that include a red-noise component. Two effects lead to this result. First, inspection of Eq (3) shows that the correlation function for a single pair of pulsars is an integral (or sum) of the products of two time series. The CLT will apply if each time series includes many independent fluctuations over the interval $[0, T]$. The sum over all pairs will also satisfy the conditions for the CLT and \widehat{C}_{00} will have a Gaussian distribution. For red noise

processes, however, each time series is dominated by of order only one fluctuation, so the CLT will not apply to the single-pair integral. The second effect is that when the CLT does not apply to the CCF for a single pair it also does not apply to the sum over all pairs, in part because a given time series contributes to $N_p - 1$ terms in the sum and the terms are not independent.

REFERENCES

- Backer, D. C., & Hellings, R. W. 1986, *ARA&A*, 24, 537
- Coles, W. A., Rickett, B. J., Gao, J. J., Hobbs, G., & Verbiest, J. P. W. 2010, *ApJ*, 717, 1206
- Cordes, J. M., & Downs, G. S. 1985, *ApJS*, 59, 343
- Cordes, J. M., & Shannon, R. M. 2010, ArXiv e-prints, arXiv:1010.3785
- Demorest, P., et al. 2009, in *Astronomy*, Vol. 2010, *Astro2010: The Astronomy and Astrophysics Decadal Survey*, 64–
- Finn, L. S., & Lommen, A. N. 2010, *ApJ*, 718, 1400
- Hellings, R. W., & Downs, G. S. 1983, *ApJ*, 265, L39
- Jaffe, A. H., & Backer, D. C. 2003, *ApJ*, 583, 616
- Jenet, F. A., Hobbs, G. B., Lee, K. J., & Manchester, R. N. 2005, *ApJ*, 625, L123
- Jenet, F. A., Lommen, A., Larson, S. L., & Wen, L. 2004, *ApJ*, 606, 799
- Lee, K., Jenet, F. A., Price, R. H., Wex, N., & Kramer, M. 2010, *ApJ*, 722, 1589
- Lommen, A. N., & Backer, D. C. 2001, *ApJ*, 562, 297
- Lyne, A., Hobbs, G., Kramer, M., Stairs, I., & Stappers, B. 2010, *Science*, 329, 408
- Manchester, R. N. 2010, *Highlights of Astronomy*, 15, 233
- Ölmez, S., Mandic, V., & Siemens, X. 2010, *Phys. Rev. D*, 81, 104028
- Ó Ruanaidh, J. K., & Fitzgerald, W. J. 1996, *Numerical Bayesian Methods Applied to Signal Processing* (Springer)
- Phinney, S. 2004, *APS Meeting Abstracts*, L9002+
- Sesana, A., Vecchio, A., & Colacino, C. N. 2008, *MNRAS*, 390, 192
- Seto, N., & Cooray, A. 2007, *ApJ*, 659, L33
- Shannon, R. M., & Cordes, J. M. 2010, *ApJ*, 725, 1607
- Smith, T. L., Kamionkowski, M., & Wandelt, B. D. 2011, ArXiv e-prints, arXiv:1104.0930
- van Haasteren, R., & Levin, Y. 2010, *MNRAS*, 401, 2372

van Haasteren, R., Levin, Y., McDonald, P., & Lu, T. 2009, MNRAS, 395, 1005

van Haasteren, R., et al. 2011, ArXiv e-prints, arXiv:1103.0576

Yardley, D. R. B., et al. 2010, MNRAS, 407, 669

—. 2011, ArXiv e-prints, arXiv:1102.2230